technical memorandum Daresbury Laboratory

DL/SCI/TM94E

THE PERFORMANCE OF PHOTOEMISSION BEAMLINE 6.1

by

P. BAILEY and F.M. QUINN, SERC Daresbury Laboratory

MARCH, 1993

993/T1

cience and Engineering Research Council

ARESBURY LABORATORY

aresbury, Warrington WA4 4AD

ISSN 0144-5677

The Performance Of Photoemission Beamline 6.1

Paul Bailey and Frances Quinn

Daresbury Laboratory

Abstract

The performance of beamline 6.1 has been characterised over several commissioning periods and the results are presented here. The monochromator covers the energy range 20 - 280 eV with an energy resolution of 0.1% of the photon energy. It has been established that a 1200 l/mm blazed grating yields higher flux with lower second order content than a 1200 l/mm lamellar grating. Three electrostatic electron energy analysers are available for use; the fixed MCD HA100 with a resolution of 1.5% of the pass energy; the fixed CMA with a resolution of 2% of the pass energy; and the HA50 on a two axis goniometer with a resolution of 1% of the pass energy. Details are also given of improvements made to the monochromator.

Table Of Contents

1. Introduction

Beamline 6.1 delivers focused monochromatic light of energy 20-280 eV into an electron energy spectrometer equipped to perform solid state photoemission studies for surface science. The Miyake geometry (reference 1) plane grating monochromator (reference 2) had previously incorporated a 632 l/mm lamellar profile grating. We report here on the performance of the monochromator using two 1200 l/mm gratings, one lamellar and one blazed.

The performance of 6.1 beamline has been assessed by quantifying (i) the monochromator flux output, resolution and order sorting efficiency and (ii) the resolution of the various energy analysers. The standard settings for performance measurements are;

the 1200 l/mm blazed grating
the grating in negative order
a 2 mm monochromator entrance aperture
the monochromator set to range 2
the exit slit set to 40 μm (100 μm micrometer reading)
a clean Cu (111) sample
a sample temperature of 110 K (for resolution measurements)
a sample temperature of 300 K (for flux measurements)
the HA100 analyser at a pass energy of 4.4 eV

1.1. A Description Of The Beamline Optics

A schematic diagram of the beamline optics is shown in figure 1 overleaf. A pre-mirror deflects synchrotron light horizontally through an angle of 11.4° onto a plane grating. The dispersed light is then focused vertically through exit slits by one of two spherical mirrors. These two mirrors provide four energy ranges as there are two focus positions for each mirror (references 2, 3), thus allowing four different included angle settings. After the exit slits, an ellipsoidal focusing mirror deflects the light horizontally through 10° to bring it to a focus at the centre of the experimental chamber. The optical elements which form the monochromator are thus; the grating, a spherical mirror and the exit slits. The wavelength (energy) of the monochromatic light is selected by rotating the grating about its horizontal axis. The monochromator is designed to be order sorting.

In this report we compare two 1200 l/mm 40 nm gold plated gratings supplied by Tayside Optical Technology; a lamellar grating with a groove depth of 13 nm and groove width 458.3 nm (nominal), and a grating blazed to an angle of 1.89°.

Details of the optical components are given in appendix 1. Monochromator settings for the four ranges are quoted in appendix 3. Instructions for changing range are given in appendix 4.

1.2. A Description Of The Spectrometer

In common with most surface science apparatus, the spectrometer is bakable to 450 K with a base pressure of 10^{-8} Pa. Samples up to 15 mm diameter are mounted on a Vacuum Generators HPLT manipulator with heating and cooling facilities. Sample cleaning by ion bombardment can be performed using a VG AG21 ion gun. Surface crystallinity can be assessed by use of a Varian 981-0127 forward-view LEED optics.

The spectrometer can use either of two fixed analysers oriented at 90° to the beam; (i) a VSW Scientific Instruments HA100 100 mm radius hemispherical analyser with an input lens (which can be retarding or accelerating) and multi channel detection and (ii) a Perkin Elmer 15-255G double pass cylindrical mirror analyser. A movable VSW HA50 50 mm radius hemispherical analyser (also with an input lens) which is rotatable in two planes can be installed at the same time as either of the above analysers. Both the HA100 and the CMA can be used to perform Auger analysis.

The technical performance of the spectrometer is detailed in appendix 11.

Figure 1: Beamline 6.1 Schematic Layout

1. Elevation

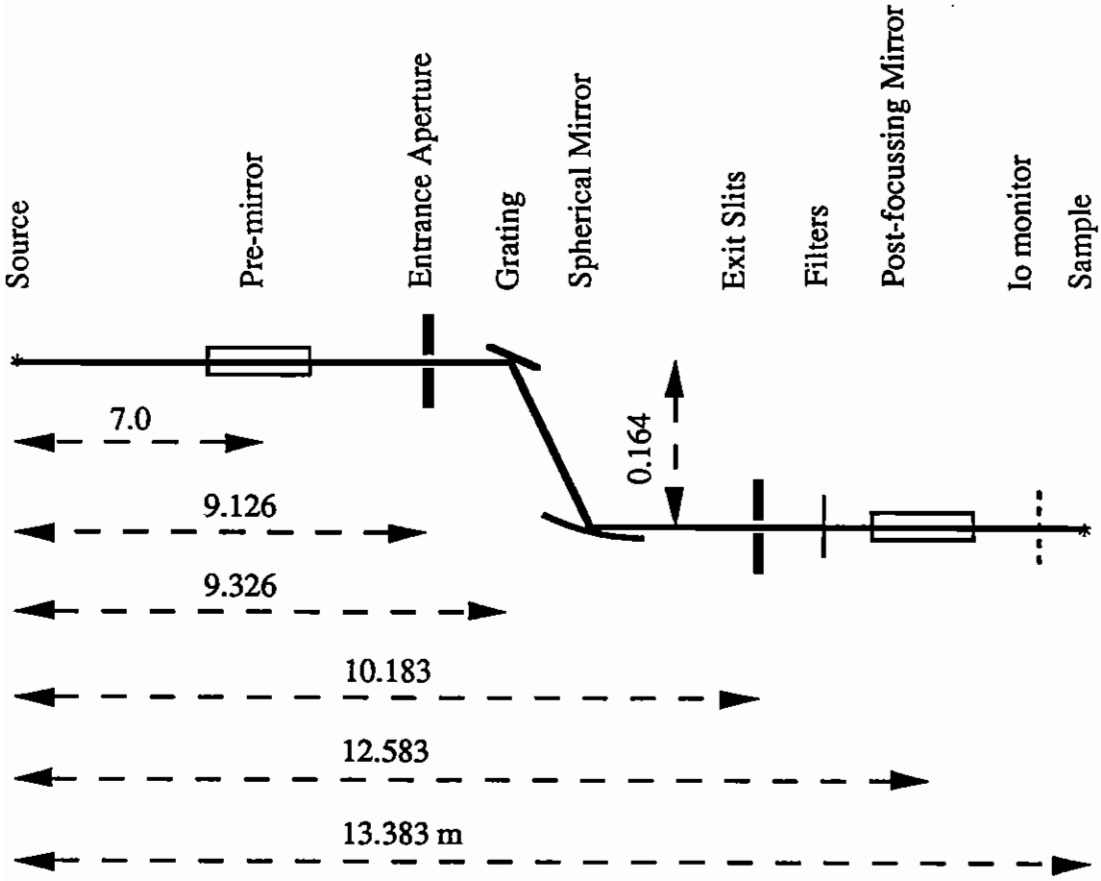

2. Plan

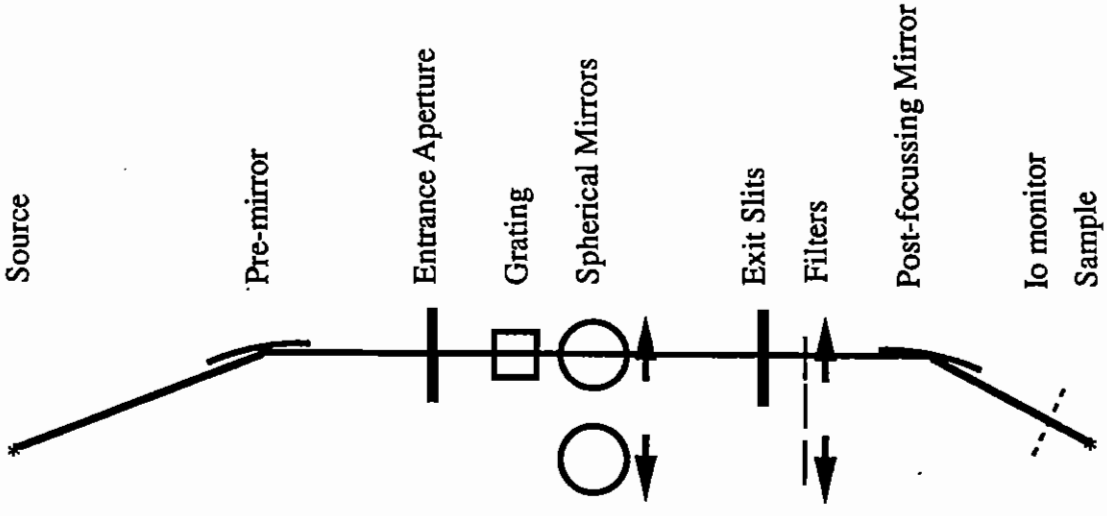

2. Monochromator performance

2.1. Flux Output

2.1.1 Measurements

Absolute flux output curves were obtained by recording the drain current from a clean copper (111) sample at room temperature and normal incidence and correcting for copper quantum efficiency using data from reference 4.

Figures 2 and 3 shows the flux curves of all four energy ranges for the blazed and lamellar gratings respectively.

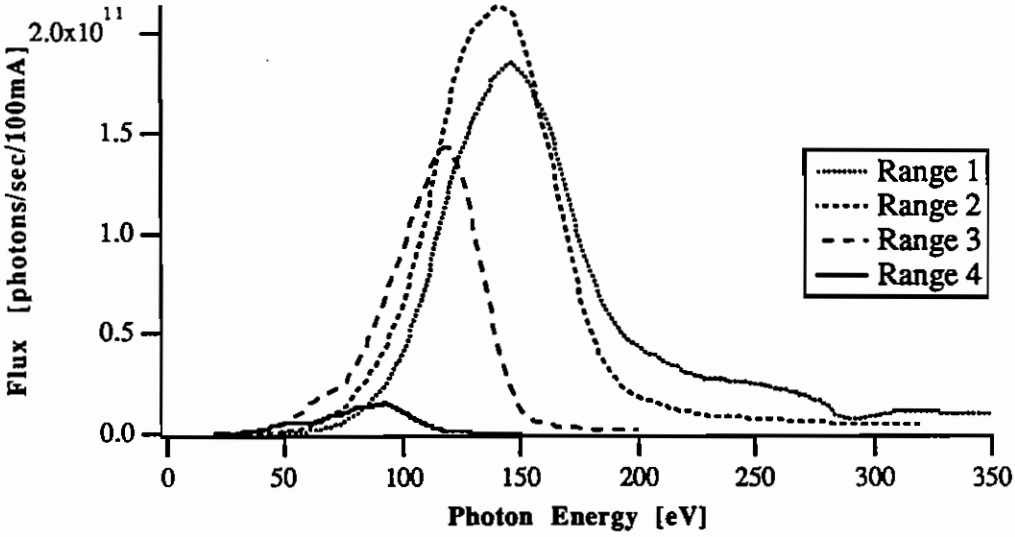

Figure 2 Flux output curves for the blazed grating (100 μm exit slit reading)

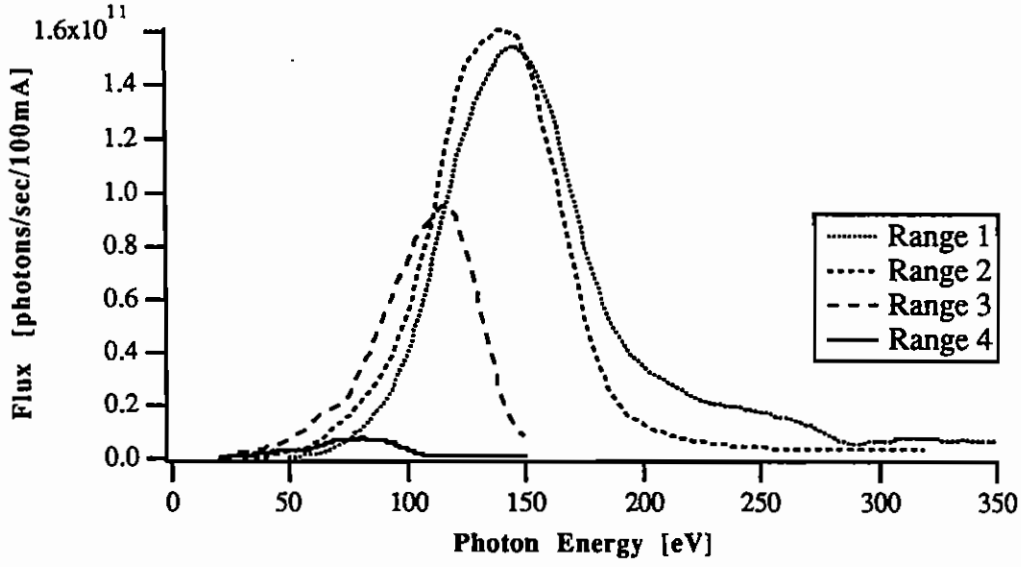

Figure 3 Flux output curves for the lamellar grating (100 μm exit slit reading)

As expected figures 2 and 3 show that the blazed grating delivers higher flux. However, it had been expected that the diffraction efficiency of the blazed grating would be about twice that of the lamellar grating (reference 5) and the measured improvement is disappointing. The blazed grating was first installed in June '91 when a

peak flux of $5x10^{11}$ photons/sec/100mA was recorded. During benchmarking in Nov. 91, this had fallen to $3x10^{11}$ photons/sec/100mA.

When it was removed from the monochromator, it was visibly contaminated and the measurements plotted in figure 2 were taken after the grating had been cleaned and recoated. It appears that the diffraction efficiency has been degraded by the recoating process.

2.1.2 Calculations

The synchrotron flux, F (photons/sec/mA/0.1% bandpass/mrad horiz.), can be calculated as a function of vertical aperture by an expression derived by Green (reference 6) for light polarsied in the plane of orbit, F_S, and out of the plane of orbit, F_P,

$$\frac{dF_s}{d\Psi} = 1.327 * 10^{13} V^2 y^2 \left(1 + X^2\right) * \left[A_h^{\,2}\right] \tag{1}$$

$$\frac{dF_p}{d\Psi} = 1.327 * 10^{13} V^2 y^2 \left(1 + X^2\right) * \left[A_v^{\,2}\right] \tag{2}$$

where Ψ is the out of plane angle in mrads, V is the machine energy in GeV, y=E/E_C with E the photon energy and E_C the critical energy in eV = 665 V^2B, B is the bending field strength in Tesla, $X = \gamma\Psi$, $\gamma = 1957$V and

$$A_h = K_{2/3}(\xi)$$

$$A_v = \frac{X}{\sqrt{1+X^2}} K_{1/3}(\xi)$$

$$\xi = \frac{y}{2}\left(1+X^2\right)^{3/2}$$

where $K_{2/3}$ and $K_{1/3}$ are modified Bessel functions of the second kind.

Several programs are available which will perform these SR flux calculations, the most convenient is SHADOW (reference 7). This can be run on VAX A or on the Daresbury SUN workstation network under the command file PACKAGE.

The reflectivity, R, of the mirror for s and p polarised light was calculated using the generalised Fresnel equations (reference 8)

$$R_s = \frac{a^2 + b^2 - 2a\cos\theta + \cos^2\theta}{a^2 + b^2 + 2a\cos\theta + \cos^2\theta} \tag{3}$$

$$R_p = R_s\left[\frac{a^2 + b^2 - 2a\sin\theta\tan\theta + \sin^2\theta\tan^2\theta}{a^2 + b^2 + 2a\sin\theta\tan\theta + \sin^2\theta\tan^2\theta}\right] \tag{4}$$

where,

$$2a^2 = \left[\left(n^2 - k^2 - \sin^2\theta\right)^2 + 4n^2k^2\right]^{1/2} + \left(n^2 - k^2 - \sin^2\theta\right)$$

$$2b^2 = \left[\left(n^2 - k^2 - \sin^2\theta\right)^2 + 4n^2k^2\right]^{1/2} - \left(n^2 - k^2 - \sin^2\theta\right)$$

where n and k are the optical constants and θ is the incidence angle.

These equations can also be expressed in terms of the atomic scattering factors f_1 and f_2 using the relations,

$$n^2 - k^2 = 1 - Df_1 \tag{5}$$

$$4n^2k^2 = \left(Df_2\right)^2 \tag{6}$$

where $D = \frac{r_0\lambda^2 N_A \rho}{\pi A}$

and r_0 is the classical radius of the electron, N_A is Avogadro's number, A is the

atomic weight and ρ is the density.

Again, several programs are available which will calculate reflectivities for a wide range of elements and compounds. These are SHADOW's utility ABREFC, Optical Constants Grapher (SF) (reference 9) and a program called ENERGY available from the Molecular Science Instrumentation project team's suite of programs. These all are based on Henke's compilation of atomic scattering factors which cover the photon energy region 100 to 2000 eV (reference 10). For platinum reflectivity below 100 eV, the above equations were used to calculate the reflectivity using the compilation of optical constants by Palik (reference 11).

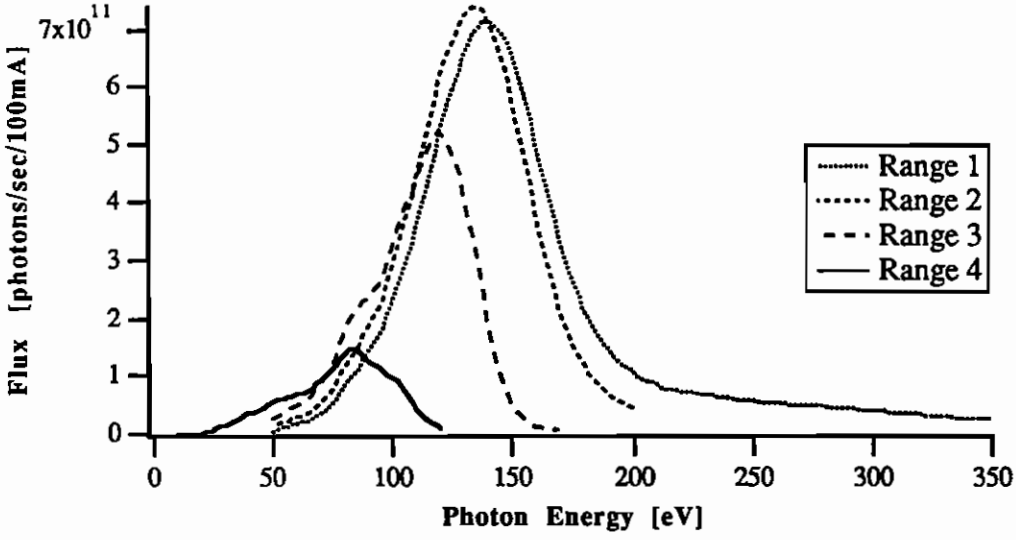

Figure 4 Calculated flux output for a lamellar grating

The diffraction efficiency for the lamellar profile grating was calculated following the method of Neviere (reference 12) using the program HUNTAEG (reference 13). This program calculates the diffraction efficiency of a lamellar profile grating as a function of energy for specified incidence angle, groove density, groove depth, groove width, and order of diffraction.

In general the shape of the calculated flux output curves and their energy range match the measurements well. However, at the maximum of range 2 the measured values are a factor of 4.5 lower than calculation. A possible explanation for this is the severe contamination of the premirror. This optical element has been exposed to SR light for many years and is visibly contaminated. But, since this element is a plane cylinder, it should be possible to simply raise this mirror vertically and so expose a clean area of mirror. Evidence of a carbon layer on the optics is also seen in the measured flux curves where there is significant drop in flux at the carbon edge.

2.2. Polarisation Calculations

Polarisation calculations can be carried out as an extension of the approach detailed above. For the optical system of beamline 6.1 consisting of a premirror M_1, a grating G, a spherical mirror M_2, and a postfocusing mirror M_3 the s polarised flux can be written,

$$F_s(\text{total}) = F_s(0.22\ \text{mrad})*R_p(M_1)*E_s*R_s(M_2)*R_p(M_3) \quad (7)$$

0.22 mrad is the vertical fan of radiation admitted by a 2 mm entrance aperture. The p polarised flux is given by,

$$F_p(\text{total}) = F_p(0.22\ \text{mrad})*R_s(M_1)*E_p*R_p(M_2)*R_s(M_3) \quad (8)$$

The degree of linear polarisation, P, is given by

$$P = \frac{F_s - F_p}{F_s + F_p} \quad (9)$$

The results of these calculations are shown in figure 5.

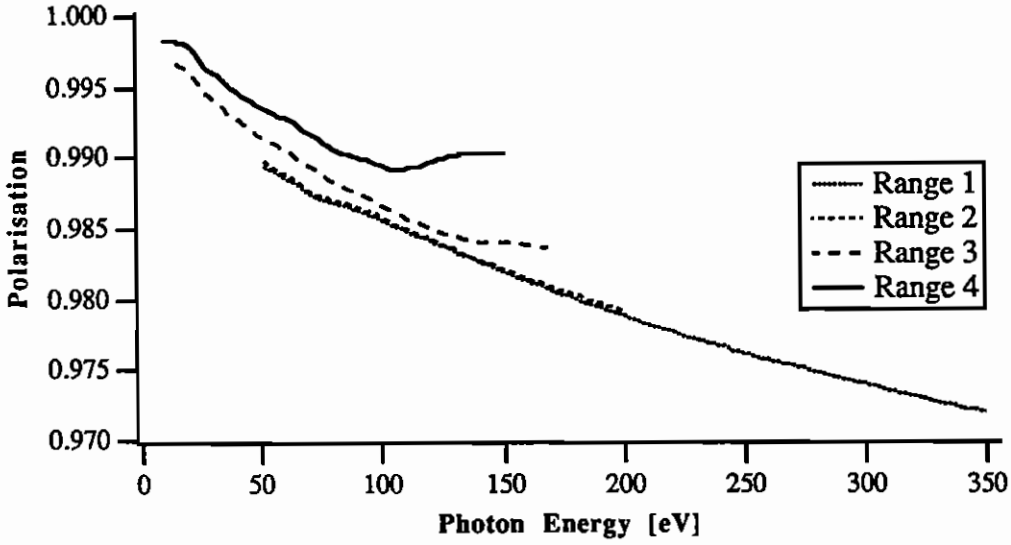

Figure 5 Calculated polarisation for 6.1

The calculated polarisation is over 97% for all ranges with the 2mm entrance aperture. As the size of the entrance aperture is increased the polarisation will fall.

2.3. Harmonic Content

2.3.1 Measurements

Harmonic content refers to the amount of higher order light contained in the monochromatic beam. Due to the order sorting design of the monochromator over the useful range of 6.1 higher orders (third upwards) are reflected inefficiently and may be ignored. To calculate the second order content we measure (i) the peak count rate from the copper valence band at the set photon energy and (ii) the peak count rate from the copper valence band produced by the second order photons. The second order content is then defined as (ii) divided by (i). Figure 6 shows the second order content (expressed as a percentage) as a function of photon energy for each of the two gratings on range 2. Figures for the second order content of the other ranges are given in appendix 10. All these figures are raw data uncorrected for the differences in copper photoemission cross-section. The actual second order content will be higher than

shown due to the general fall in cross-section with photon energy.

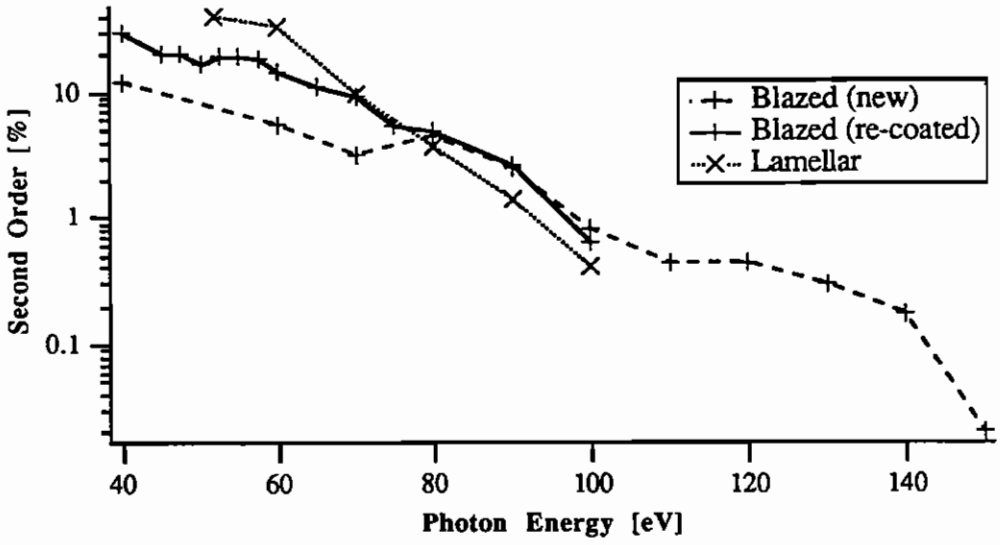

Figure 6 Second order content

It can be seen in figure 6 that below 80 eV the lamellar grating produces more second order than the blazed grating and produces a similar amount above 80 eV. This is contrary to the behaviour noted in reference 14. The difference in figure 6 between the new and re-coated grating agrees with section 2.1.1 in indicating that re-coating the grating has affected its performance.

2.3.2 Filter Efficiency

The amount of second order content shown in figure 6 can present difficulties for certain experiments at lower photon energies. The second order can be reduced significantly by transmission through a thin metal film whose absorption edge lies at a favourable photon energy. Figure 7 shows the effectiveness of three different filters supplied by Luxel corp. whose compositions are (i) a 120 nm film of silicon, (ii) a 150 nm film of aluminium and (iii) a sandwich of 50 nm Al, 200 nm Mg and 50 nm Al. These are supported on a 82 % transmission Ni mesh. In figure 7 the filter efficiency is defined as the ratio of the fractional second order content (defined above) with the filter in place to that with no filter in place.

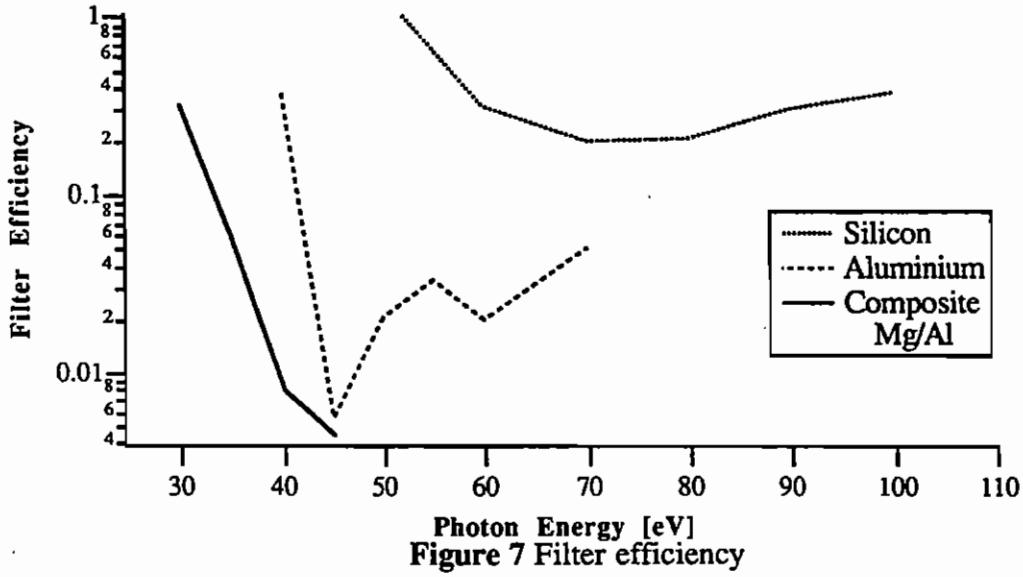

Figure 7 Filter efficiency

Figure 8 shows the experimentally determined transmission of the filters. The transmission is defined as the ratio of the copper valence band maximum with and without the filter in place. More information can be found in reference 15. The operational settings of the filters are given in appendix 6.

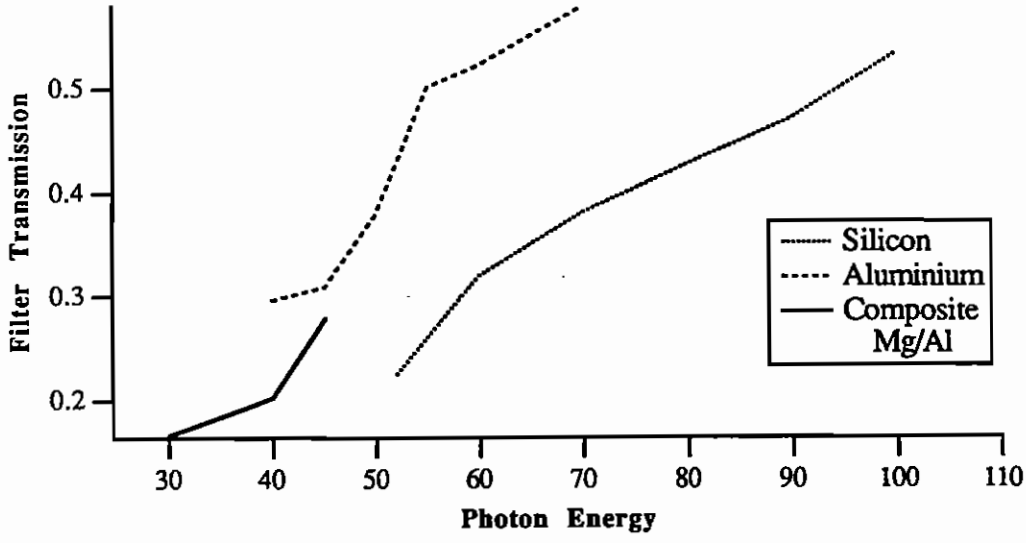

Figure 8 Filter transmission

From figures 7 and 8 one may deduce the useful operational range of each filter. These figures are given in appendix 6.

2.4. Resolution

The ultimate resolution of the monochromator is determined by the source size limited resolution, σ, in eV;

$$\sigma = \frac{sE^2 \cos\alpha \times 10^7}{NL \times 12398.5}$$

where s is the vertical source size in mm, E the photon energy in eV, N the line density of the grating in lines/mm, L the grating to source distance (9326 mm) and α the incidence angle on the grating. There are three variable parameters which also affect the resolution; the monochromator entrance aperture, the focus position of the spherical mirror and the monochromator exit slit size. The monochromator resolution has been characterised by measuring the resolution as a function of these parameters.

2.4.1 Experimental method

The resolution of the monochromator was determined by energy analysing the photoelectron yield from a clean copper (111) sample around the region of the Fermi edge. For most measurements the sample was cooled to 110 K and oriented at 45° to the photon beam. The energy analyser used was the HA100 operating at a pass energy of 4.4 eV. These figures give an analyser resolution of 64 meV, a Gaussian equivalent of the Fermi width of 33 meV and hence, a combined resolution of 72 meV.

2.4.2 Deconvolution technique

The widths of experimental Fermi edges were determined by our own curve fitting routine using the 'Igor' data analysis package on an Apple Macintosh IIci computer (reference 15). The expression used was the sum of four terms; (i) a constant background level, (ii) an exponential term which is zero beyond the Fermi edge, (iii) an

second exponential term which is non-zero beyond the Fermi edge, and (iv) an ideal Fermi edge from which the edge width is derived. The physical basis of each of these terms is as follows;

(i) the analyser we used tends to give a constant background level which we believe is a result of its retarding lens transmitting a small amount of off axis electrons

(ii) this term matches the general fall in the density of states as one nears the Fermi edge

(iii) since there are no occupied states above the Fermi edge the yield in this region should be zero. However higher order light will produce electrons in this region and the general spectrum will be that of a secondary tail, i.e. exponential in form

(iv) if one had perfectly monochromatic light the electron yield would be of the form of an ideal Fermi edge. In practice, this is convolved with the analyser transmission function and the monochromator transmission function. As it can be shown that a Fermi edge convolved by a Gaussian function retains its characteristic shape and we expect the transmission functions to be approximately Gaussian we are justified in using an ideal Fermi edge in our fit. The fact that we obtain a good fit using an ideal Fermi edge validates our assumptions. A limitation of this approach is the perturbing effects of other photoemission features in the region of the Fermi edge. These may be due to first or second order light and so may appear above or below the edge.

Figure 9 shows the fit to an experimental Fermi edge with relatively poor signal to noise ratio.

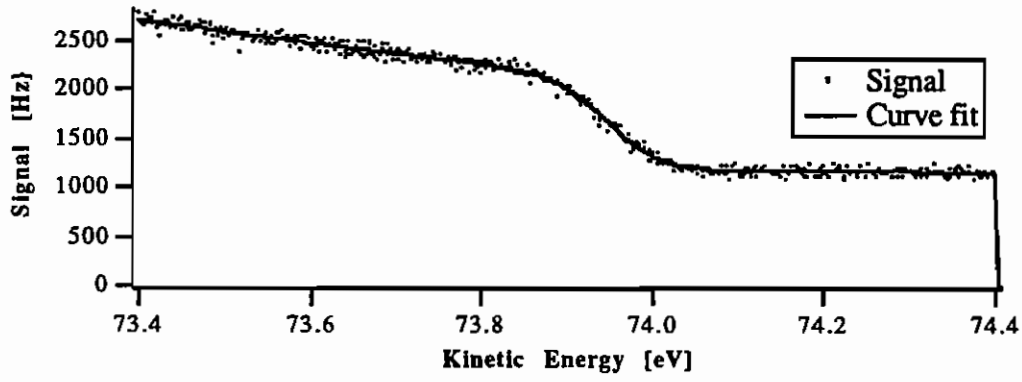

Figure 9 Illustration of a Fermi edge curve fit

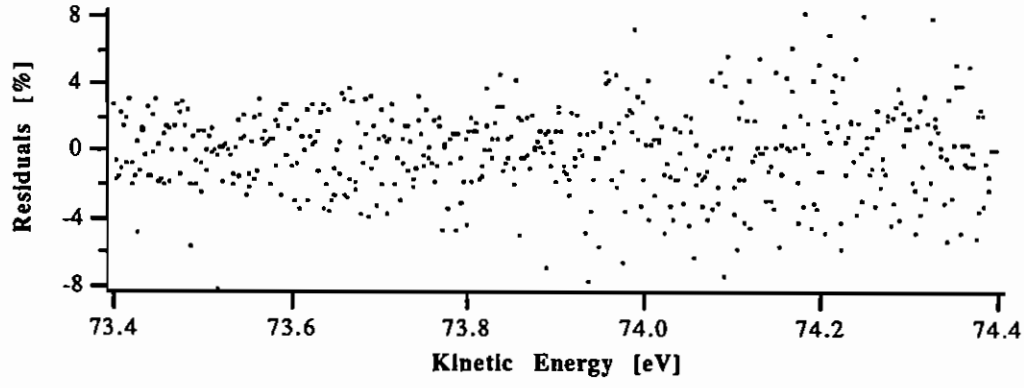

Figure 10 The difference spectrum from figure 9

A plot of the difference between the signal and the fit in figure 10 shows that there is no particular region of mismatch.

As the derivative of a Fermi function can be approximated by a Gaussian we can convert the Fermi edge 'temperature' value produced by part (iv) of the curve fit to

an equivalent Gaussian FWHM simply by multiplication of a constant (3.038×10^{-4} to give a result in eV from a temperature in K). The monochromator bandpass is then obtained by subtracting in quadrature the contributions due to the analyser and thermal broadening of the Fermi edge (given in section 2.4.1 above).

2.4.3 The Effect Of Focus Position

The function of the spherical mirror is to focus the monochromatic light at the exit slits. As focus position is a function of the photon energy, the mirror will only focus at the exit slits for one photon energy (reference 17). Other energies will focus before or after the slits and so have a degraded energy resolution. By altering the included angle of the monochromator it is possible to set the in-focus energy to a predetermined value (reference 18). This is normally set to focus at 154 eV, in the middle of the most frequently used photon energy range. We have measured the dependence of the monochromator resolution on the mirror to exit slit distance at mirror positions either side of the theoretical 154 eV focus position for the photon energy corresponding to peak flux on range 2, i.e. 140 eV. The measurements were taken using an exit slit micrometer reading of 20 μm, an analyser pass energy of 4.4 eV (64 meV linewidth) at room temperature (89 meV Fermi width). The monochromator bandpass was obtained from the experimental Fermi width by subtracting in quadrature the contributions due to the analyser and thermal Fermi edge broadening. The results tabulated below show that the calculated focus position does give the best resolution.

Mirror to slit distance, mm	Mirror Translate Cyclometer, MT	Resolution @ 140 eV, meV
361.8	4445	275
354.1 (154 eV focus)	4545	176
346.5	4565	195

The benefit of operating the monochromator in focus at 154 eV is shown in figure 11. This compares the resolution as a function of photon energy for focus at zero order to focus at 154 eV. The resolution is a factor of two lower in the latter case over the usable range of 6.1. Also plotted are the predictions of SHADOW for each focus position. The data were acquired in November '91.

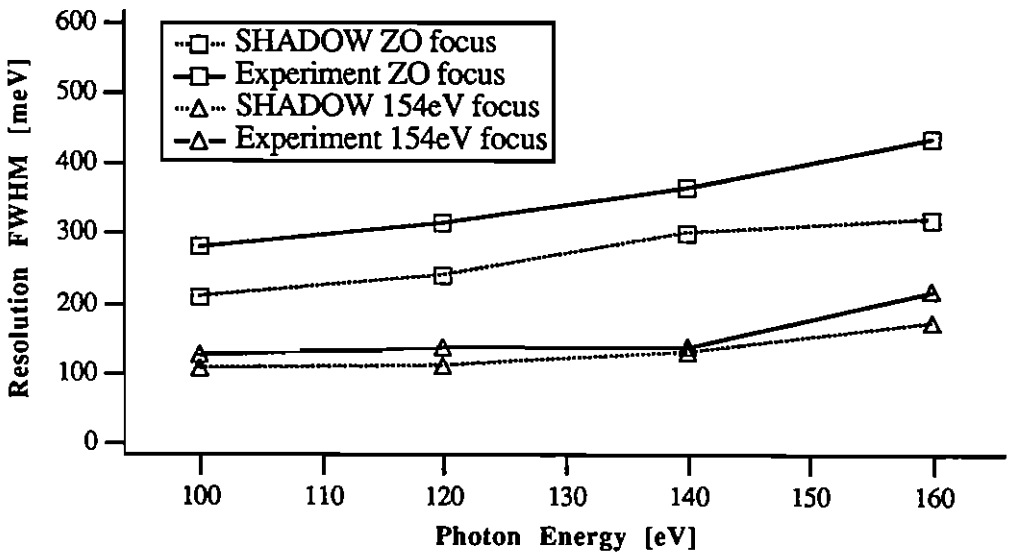

Figure 11 Effect of changing the monochromator included angle to focus at 154 eV (ZO refers to the zero order focus position)

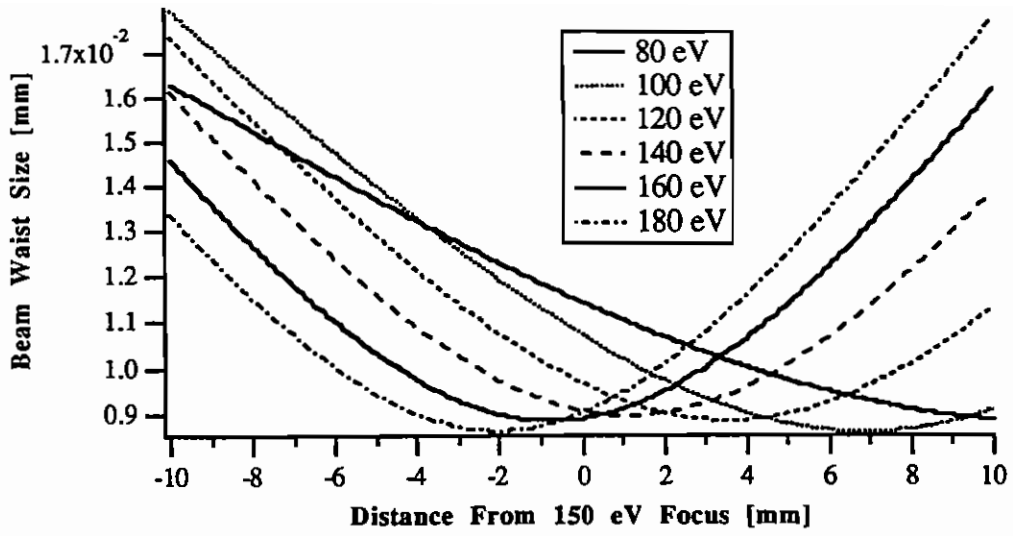

Figure 12 Beam waist size vs. focus position

In figure 12 the focused beam waist size found using SHADOW (reference 7) is shown as a function of position for a range of energies.

The distance quoted in figure 12 is the distance from the 154 eV focus position with positive distances referring to positions further from the tangent point. The position of the spherical mirror in relation to the exit slits has a strong effect on the observed resolution: thus it is essential to choose a position suitable for the energies of interest. It can be seen that typically a 10 mm shift near the beam focus results in a 50% increase in beam size.

2.4.4 The Effect Of Entrance Aperture Size

This type of monochromator is referred to as entrance slitless, i.e. it images the source not an entrance slit. However it has an entrance aperture which limits the beam size on the spherical mirror and hence determines the amount of coma and other aberrations produced in the dispersing direction. The entrance aperture lies about 0.2 m in front of the grating and consists of a movable aperture rack with 6 apertures varying in 1 mm steps from 1 to 6 mm. The usual aperture size is 2 mm which admits a 0.22 mrad vertical spread of light into the monochromator. We have measured the resolution as a function of this aperture size and the results are shown in figure 13. Range 3 was chosen since on this range a 6 mm aperture just fills the grating.

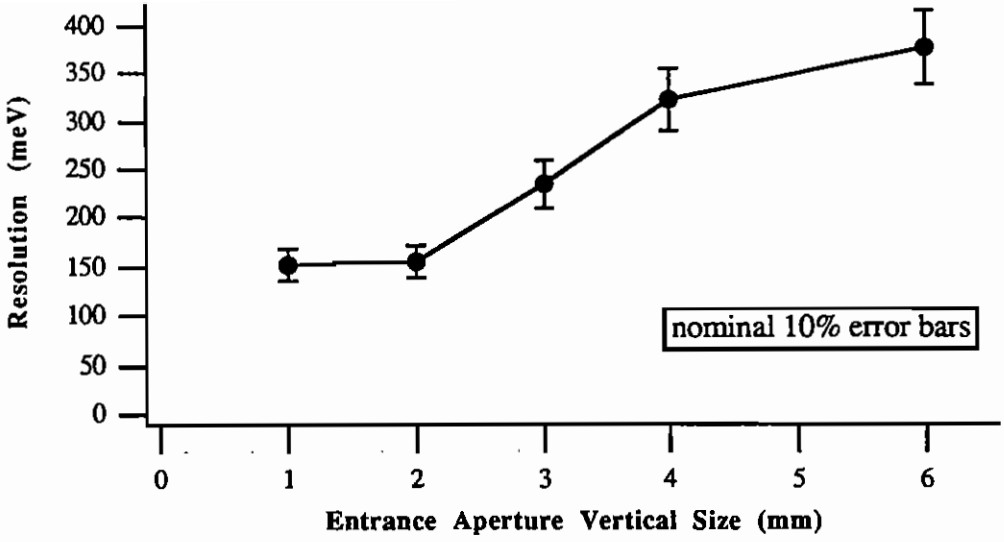

Figure 13 Effect of entrance aperture size on resolution (for range 3 at 100 eV)

It can be seen that the entrance aperture size has a noticeable effect on resolution for range 3. The resolution broadening caused by widening the entrance aperture is due to increased coma and defocus. Similar effects are seen for the other three ranges up to the point when the grating is fully illuminated. The entrance aperture size also affects the throughout (flux) of the monochromator and the degree of polarisation. For the range of aperture sizes described here the flux is proportional to the aperture size and, as was was noted in section 2.2, increasing the entrance aperture size will lower the polarisation. The following table gives the entrance aperture size which will completely illuminate the grating when at the zero order angle.

Range	Aperture size, mm
1	3.0
2	3.8
3	6.2
4	9.9

2.4.5 The Effect Of Exit Slit Size

The monochromator exit slits limit the monochromator exit beam size in the dispersing direction (vertically). Thus their size affects both the resolution and the throughput (flux) of the monochromator. We have measured the energy resolution at a number of photon energies for a range of exit slit sizes and the results are shown in figure 14.

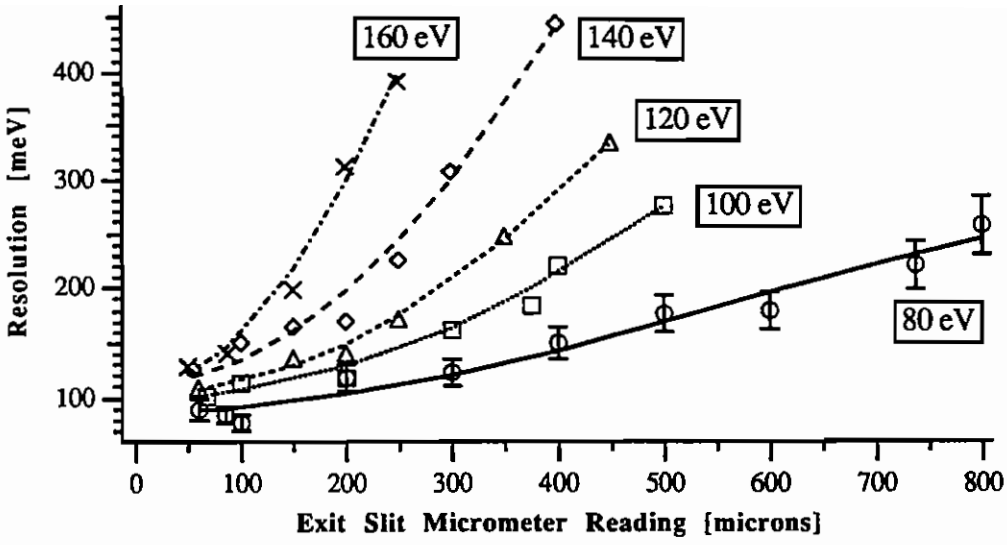

Figure 14 Resolution as a function of exit slit micrometer reading (for range 2)

The exit slit micrometer reading is a factor of 2.5 greater than the actual slit width. The curves drawn through the data points in figure 14 are Gaussian in form and their values are given in appendix 7 as an aid to interpolating between the experimental points. It is noticeable that some of the resolution vs. exit slit data appear to be outside the normal error range and we suspect that there may be some experimental problem which will require further investigation. The resolutions of the lamellar and blazed gratings at the theoretical source size limited slit settings match to within 5%. The resolution at our usual exit slit micrometer reading of 100 μm corresponds to a 0.1 % bandpass across the energy range 80 to 160 eV.

For comparison figure 15 shows the equivalent SHADOW raytracing predictions (the topmost curves).

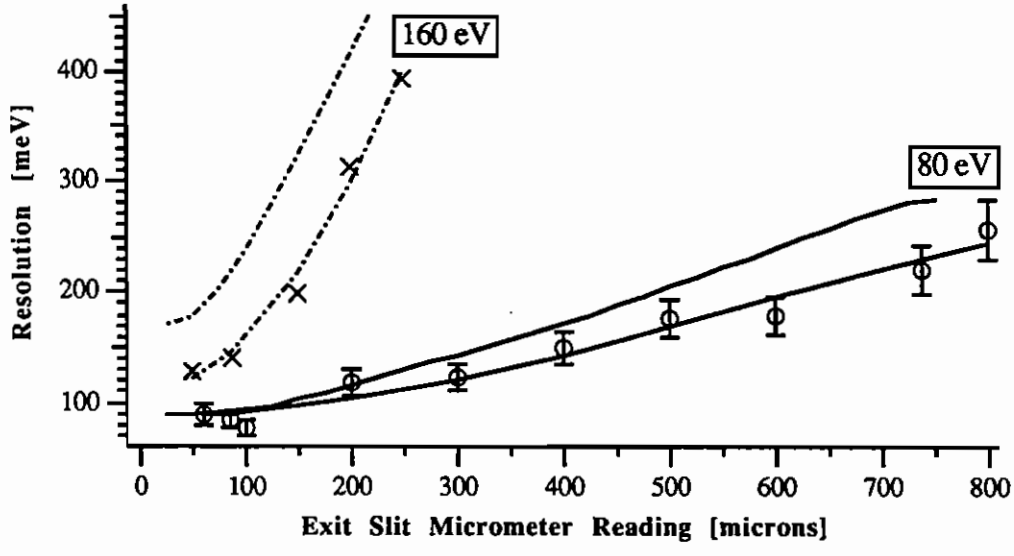

Figure 15 Comparison of simulated and measured resolution

Measurement and prediction agree well for 80 eV photon energy. For other energies, the shape of the curves are in reasonable agreement but the quantitative agreement is poor and gets progressively worse for higher energies. At 160 eV, the simulation is typically 50% higher than experiment.

The data shown in figure 14 allow us to predict the exit slit settings required to produce a fixed bandpass across a given photon energy range. The fixed bandpass curves shown in figure 16 are an exponential fit to data points interpolated from figure 14. The empirical expressions for the fit are given in appendix 8. It can be seen that these expressions are accurate to the data within about 10%.

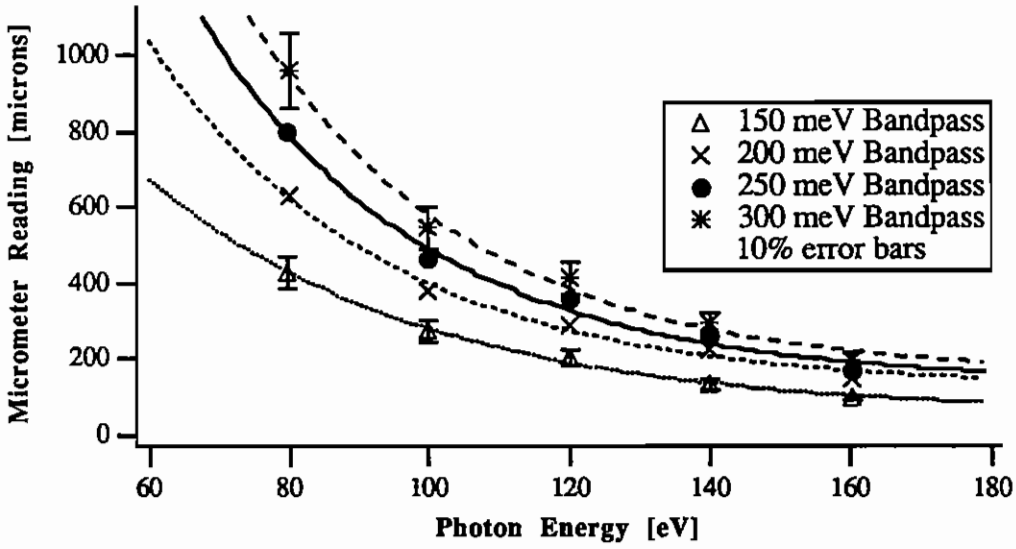

Figure 16 Exit slit micrometer readings for fixed bandpass

Figure 17 shows the variation in flux as a function of exit slit width. At the wider slit settings both flux and resolution are approximately linear with slit size.

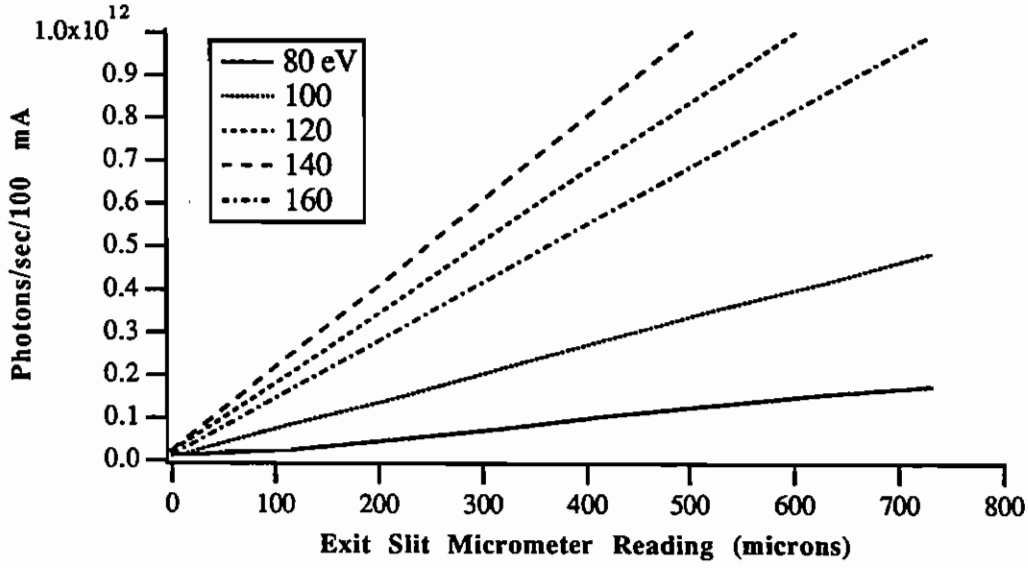

Figure 17 Flux as a function of exit slit micrometer reading

It is apparent from figures 14 and 17 that choice of exit slit size represents a trade-off between flux (throughput) and resolution. This choice can be quantified by combining the data from figures 14 and 17 to produce a 'goodness' factor for the beamline which we define as the ratio of flux to bandwidth at a fixed exit slit setting. Figure 18 shows the goodness factor for beamline 6.1 plotted vs. exit slit reading. The units of the 'y' axis are photons/sec/100 mA/meV.

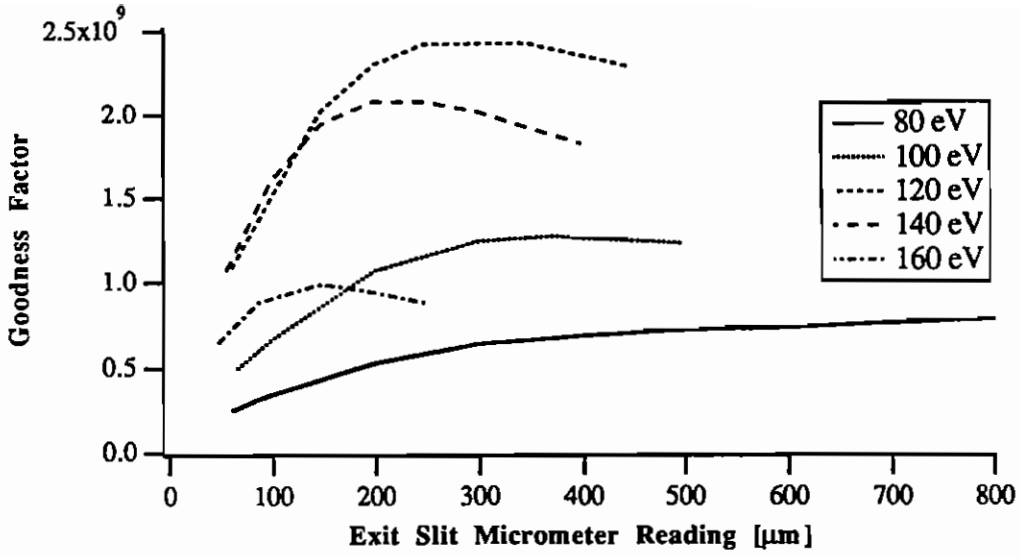

Figure 18 Goodness factor for 6.1 beamline on range 2
(the units of the 'y' axis are; photons/sec/100 mA/meV)

An interesting feature of figure 18 is the position of the peaks in relation to our usual exit slit size of 100 μm. It is evident that a slit of 150 or 200 μm would place the operating point much closer to the peaks of the goodness curves. In fact we predict that increasing the exit slit from 100 to 150 μm will increase the flux by 50% and result in an increase in bandpass from 0.1% to 0.12% over the range 80 to 160 eV. An increase to 200 μm begins to compromise the 160 eV resolution.

3. Electron Energy Analysers

3.1. HA100

The VSW Scientific Instruments MCD HA100 electrostatic energy analyser is an angle resolving 100 mm radius hemispherical analyser with a retarding/accelerating input lens. Using the HAC5000 control unit, either electrons or ions can be analysed. The detector consists of chevron channel plates with 16 anode strips which allows simultaneous multichannel detection. The VSW HA100 resolution has been tested to investigate its suitability for PES on VUV 6.1.

The lens has been raytraced with SIMION4 (reference 19) to enable the theoretical resolution limit to be calculated.

The resolution of a hemispherical analyser is given by,

$$\frac{\Delta E}{E_0} = \frac{0.43}{R_0}\left[\frac{s_{en} + s_{ex}}{2}\right] + 0.25\alpha_{an}^{\ 2} \qquad (11)$$

where E_0 is the pass energy, R_0 is the mean radius, s_{ex} and s_{en} are the exit and entrance slit sizes in the dispersive plane and α_{an} is the half-angle of the electron beam as it enters the hemispheres (reference 20).

For this analyser, R_0 is 100mm, s_{ex} is 1.44mm (the anode spacing), and s_{en} can be 1mm, 2mm, 4mm, or 5mm. SIMION was used to determine α_{an} and α_s (the maximum angle from the axial source point which is transmitted by the lens. The results are summarised below.

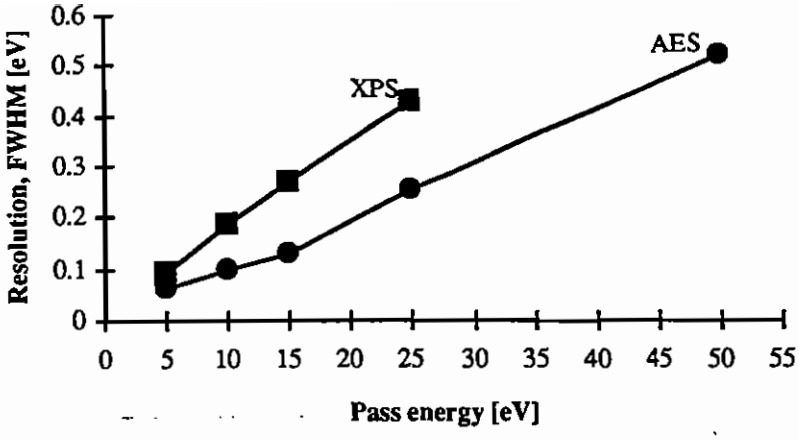

Figure 21 CMA resolution as a function of pass energy for the AES and XPS apertures

Figure 22 shows a comparison of the two operational methods which give a similar resolution; using a large aperture and low pass energy, and a small aperture and higher pass energy. It is obvious that using a larger aperture and low pass energy gives better performance for UPS.

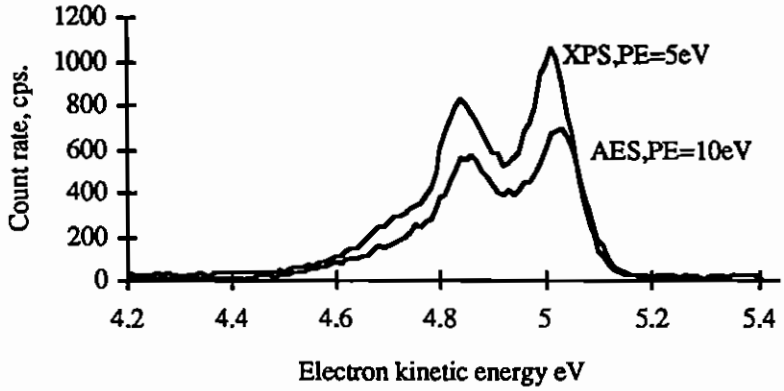

Figure 22 Comparison of two spectra with nearly equivalent resolution showing the relative effects of the aperture size and the pass energy on the count rate.

Because of the orientation of the lamp, gas jet and analyser, the source is effectively a flooded source; using synchrotron radiation , SR, the source will only be partially flooded to a degree dependent on the retardation. The retardation by the hemispherical grids in this experiment = KE/PE varies from 1 to 0.1. This is more usually 2 to 10 using SR (KE = 40 to 100 eV; PE = 10 to 25 eV)

4. Conclusions

The flux output and resolution of the beam line are in general agreement with calculations. The factor of 4.5 loss in intensity may be ascribed to the fact that the pre-mirror is highly contaminated due to its long exposure to synchrotron light. At 100 μm exit slit reading the resolution of the monochromator is approximately 0.1% of the photon energy.

The blazed grating gives slightly higher flux than the lamellar with lower second order content. Since the resolution figures are very similar we have decided to designate the blazed grating for normal routine use and keep the lamellar grating in reserve for occasions when the blazed one may require recoating.

At the lower photon energies where the second order content may become a

problem there are three filters which can be used to preferentially attenuate the higher orders. On range 2 these will limit the second order to less than 1%.

As expected the position of the spherical mirror in relation to the exit slit has a strong effect on the resolution due to its focusing effect. The results show that it is most important to set up the monochromator at the correct focus position for each energy range.

The HA100 resolution at 1.5% of the pass energy is significantly poorer than the theoretical limit. This needs to be investigated. However, the overall performance in terms of count rate and resolution is still better than the CMA, and it is recommended as the usual analyser for this station. The CMA resolution is not sufficiently good to allow the benefits of the higher resolving power of the monochromator to be fully exploited.

The rotatable HA50 angle resolving analyser performs as expected with a resolution of 1% of the pass energy.

The CMA also performs as expected with a resolution of 2% of the pass energy.

5. Recommended Improvements

In order to increase the flux output of the beamline the pre-mirror will be raised so as to illuminate a clean area of mirror surface. Calculations indicate that a factor of 4.5 improvement is possible for a lamellar grating. A blazed grating should be capable of a further factor of 2.

Computer control of the exit slit mechanism will be implemented so that fixed bandpass scans can be carried out. The quantification of the effect of exit slit size on resolution described here now makes this possible.

A quantitative photodiode will be installed immediately after the exit slits. Benchmarking of flux output will then be possible without the need for a clean copper sample and the attendant lengthy preparation time.

Further simulations and experiments will be carried out to resolve the difference between predicted and measured resolution at the higher photon energies.

Future experiments will be conducted to characterise ranges 1, 3 and 4 at non-zero order focus positions.

6. Recommended Operating Procedure

The usual operational exit slit micrometer reading of 100 μm should be increased to 150 μm. The flux output will then increase by 50% whilst the bandpass will only increase by 20% from 0.1% to 0.12% of photon energy. The exit slit size for a specific resolution is given in appendix 7.

The maximum entrance aperture size which allows the desired resolving power should be used to optimise the flux.

Careful alignment of the monochromator and entrance aperture is essential for optimum resolution.

Careful alignment of the zero order light is essential for optimum resolution.

Careful alignment of the HA100 by eye (not maximising count rate) is essential for good analyser performance.

The analyser resolution should not differ from the monochromator resolution by more than a factor of two.

The appropriate second order filter should be used at photon energies below 100 eV.

References

1. Miyake K.P. Kato R. and Yamashita M. Sci.Light **18** (1969) 39
2. Howells M.R., Norman D., Williams G.P., and West J.B., J.Phys E **11** (1978) 199
3. Padmore H.A., Daresbury Lab. Tech. Memo. DL/SCI/TM 45 E (1986)
4. Day R.H., Lee P., Saloman E.B. and Nagle D.J., J.App.Phys **52**(11) (1981) 6965
5. Neviere M. and Flamand J., Nucl.Inst. and Meth. **172** (1980) 273
6. Green K. in 'Reference documents for a national synchrotron light source' ed. Blewett J.P., BNL 50595 Vol 2,
7. Welnak C., Anderson P., Khan M., Singh S. and Cerrina F., Rev.Sci., **63** (1992) 865
also Lai B. and Cerrina F., Nucl.Inst. and Meth. **A246** (1986) 337-341
8. West, J.B. and Padmore H.A., Daresbury Lab. Tech. Memo. DL/SCI/P536E (1986) also in 'Handbook of Synchrotron Radiation', Vol 2
9. Optical Constants Grapher, Mark Thomas, Centre for X-ray Optics, Lawrence Berkeley Laboratory.
10. Henke B.L., Lee P., Tanaka, T.J., Shimabukuro R. and Fujikawa, B.K., Atomic and Nuclear Data Tables, **27**, (1982)
11. Palik, E.D. 'Handbook of Optical Constants' Academic Press (1985) (note there is an error in the energy column for the Pt table, 45.59 eV should read 49.594 eV)
12. Neviere M., Nouv.Rev.Optique, **5**, (1974) 65
13. HUNTAEG, Core supplied by M.Neviere, extensions written by H.A.Padmore
14. Neviere M., Flamand J. and Lerner J.M., Nuc.Inst. and Meth. **195** (1982) 183
15. Quinn F.M., Bailey P. and Teehan D., Daresbury Lab. Tech. Memo. DL/SCI/TM91E (1993)
16. IGOR, WaveMetrics Inc., PO Box 2088, Lake Oswego, OR 97035, USA
17. Murty M.V.R.K., J.O.S.A. 52 (1962) 768
18. Quinn F.M. and Bailey P., Daresbury Lab. Tech. Memo. DL/SCI/TM89E
19. Dahl D.A., Delmore J.E. and Appelhans A.D., Rev.Sci.Instr. **61** (1990) 607
20. Imhof R.E., Adams A. and King G.C., J.Phys.E, Sci.Instr. **9** (1976) 138
21. Palmberg P.W., J.Elec.Spec. and Rel.Phen., **5** (1974) 691-703

Acknowledgements

The authors wish to thank Dr. H.A. Padmore for many useful discussions during the course of this work.

Appendices

A.1 Optical Elements

Quoted distances are measured horizontally

iris plate;	distance to source	6.61 m
	distance to pre-mirror	0.39 m
	active area	0.1856 x 0.033 m
pre-mirror;	distance to source	7 m
	distance to entrance aperture	2.126 m
	horizontally focusing cylinder	4.677 m radius
	incidence angle	84.53°
	active area	0.56 x 0.05 m
	material	SiC
	coating	30 nm Pt
entrance aperture;	distance to source	9.126 m
	distance to grating	0.2 m
	active area	20 mm horizontal
	size	from 1 to 6 mm vertical
	material	stainless steel
grating;	distance to source	9.326 m
	distance to spherical mirror	variable (0.3541 m @ R2 154 eV focus)
	plane blazed grating	1200 l/mm, 1.89° blaze angle
	included angle	Range 1; 165.918°
		Range 2; 161.9° (@ R2 154 eV focus)
		Range 3; 150.466°
		Range 4; 132.08°
	active area	25 x 25 mm
	material	spectrosil
	coating	40 nm Au
spherical mirrors;	distance to grating	variable (0.5029 m @ R2 154 eV focus)
	distance to exit slit	variable (0.3541 m @ R2 154 eV focus)
	radii	3.25 or 4.206 m
	active area	35 mm diameter
	material	spectrosil
	coating	40 nm Au
exit slit;	distance to grating	0.857 m
	distance to postmirror	2.4 m
	active area	20 mm horizontal
	size	from 4 to 400 mm vertical
postmirror;	distance to exit slit	2.4 m
	distance to sample	0.8 m
	incidence angle	85°
	ellipsoidal radii	1.6 and 0.1207 m
	active area	0.5 x 0.046 m
	material	spectrosil
	coating	50 nm Au

A.2 Alignment of Zero Order Light

Careful alignment of the zero order beam on the spherical mirror is essential for obtaining good resolution. As the monochromator is operated with the focus at 154 eV, the zero order image is defocused. Also, to simply optimise the grating angle and mirror rotation for maximum drain current on I_0 can lead to serious misalignment of the image on this mirror.

Rocking curves can be taken to assess the zero order image width. These are done by using the CAL option in the ADES menu. Drain current from the I_0 grid or a sample is recorded as a function of encoder position. One press of the < and > keys is equivalent to one stepper motor step which is in turn equivalent to about 1.28 encoder units. Hence, if the grating angle is moved one step at a time, the encoder reading will increase one unit at a time with occasional increases of two units.

Figure 23 shows a rocking curve using MT settings for focus at 154 eV (an included angle of 161.9°) after systematically optimising GC and then MR to obtain maximum flux. The drain current was measured from a clean Cu (111) sample at normal incidence using a narrow exit slit of 20 μm micrometer reading. The curve looks quite sharp and symmetrical, but when the image was checked it was found to be on the upstream edge of the mirror. The resolution at 140 eV under this condition was 400 meV (using an exit slit reading of 22 μm, equivalent to source size, and an entrance aperture of 2 mm).

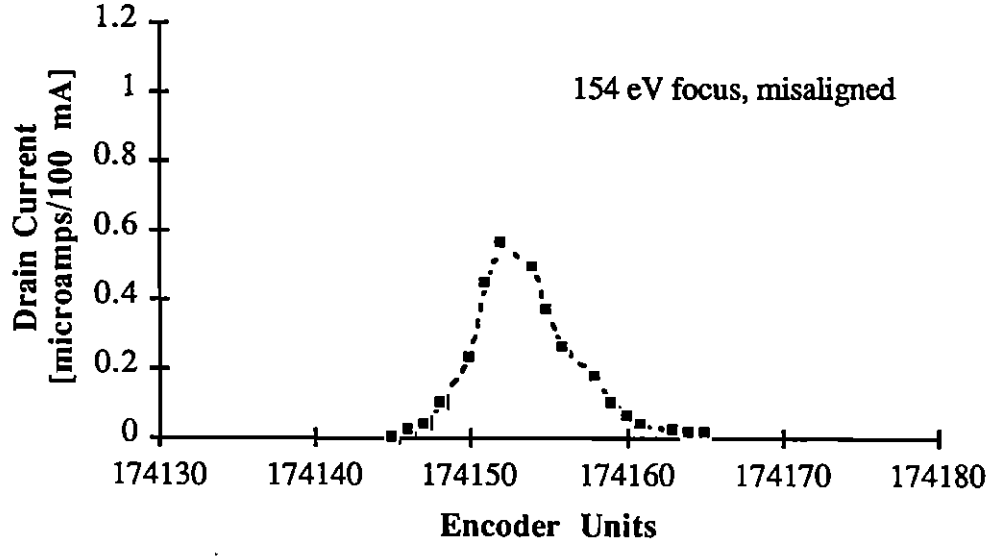

Figure 23 Rocking curve obtained with the monochromator included angle of 161.9°

The second curve, figure 24, was recorded after aligning the zero order image centrally on the mirror with no aperture in, and then winding the aperture in centrally using the image on the mirror as a reference. The resolution at 140 eV was then 224 meV.

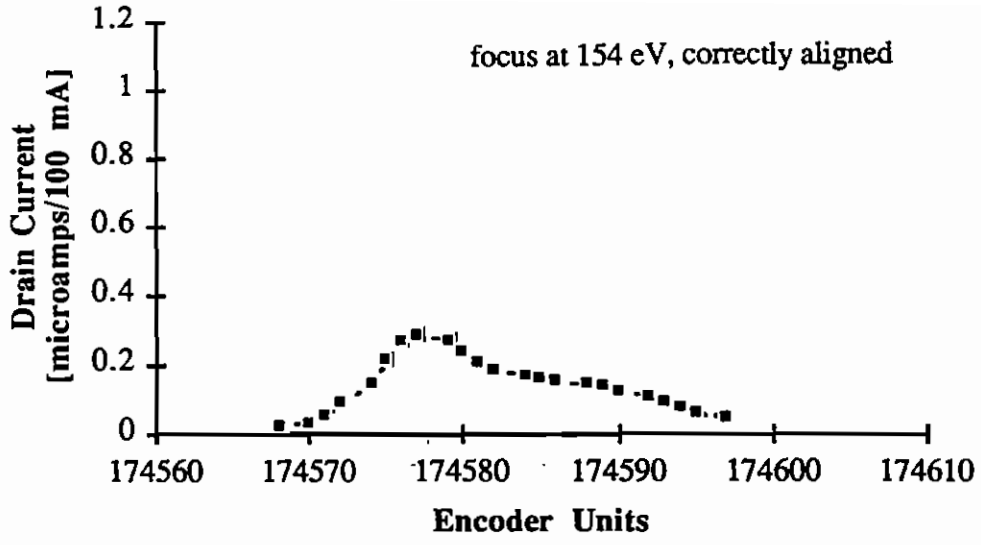

Figure 24 Rocking curve with zero order light central on the mirror

Figure 25 shows the rocking curve obtained with the monochromator included angle of 162.976°, which gives the focus at zero order. The image is obviously much sharper than at the previous setting, but the resolution at 140 eV was 392 meV.

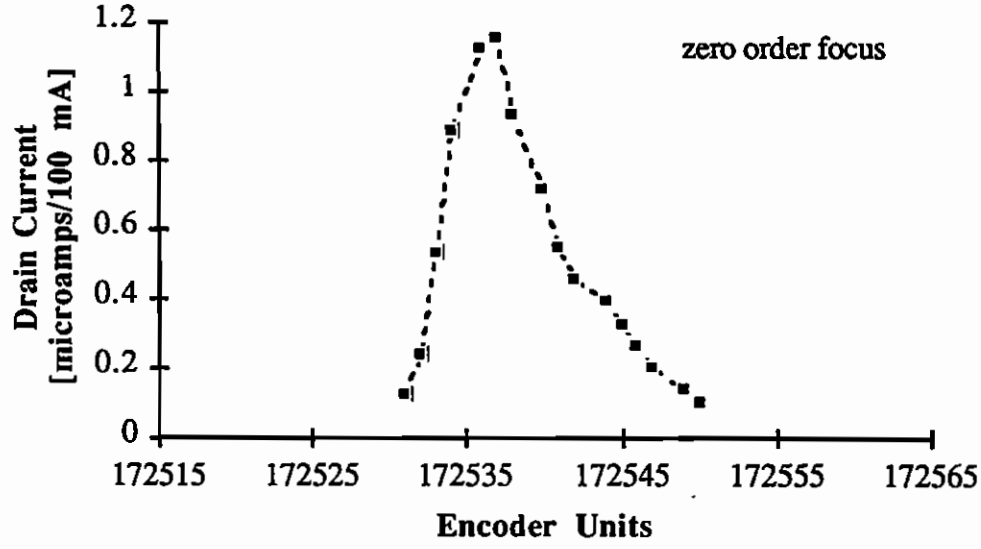

Figure 25 Rocking curve for zero order focus settings

A.3 Monochromator Settings

The following table is a list of the latest (Sept. '92) operational settings for each energy range. MT is the mirror translate cyclometer reading which indicates the horizontal position of the spherical mirror. MR is the mirror rotate cyclometer reading indicating the angle of rotation of the mirror. GC is the grating cyclometer reading and GE is the grating encoder reading as read by the station computer, both of which indicate the angle of rotation of the grating.

Range	MT cyclometer @ focus energy	MR cyclometer	GC cyclometer	GE reading
1	6534 (ZO)	919327	827	16877
2	4545 (154 eV)	918823	1875	174499
3	1755 (ZO)	917282	2020	196382
4	-103 (ZO)	914755	3393	231530

ZO refers to the zero order focus position.

The following table lists a number of useful MT readings against actual spherical mirror position;

Range	Focus energy eV	MT cyclometer	exit slit dist. mm	dist. to flange mm
1	ZO	6534*	203.2	40.45
1	180	6394	213.6	50.85
2	ZO	4976	321.3	158.55
2	154	4545	354.6	191.85
3	ZO	1755*	567.3	404.78
4	ZO	-103	708.9	546.15
4	60	18.5	699.7	536.95

Again ZO refers to the zero order focus position. The figures above marked with an asterisk (*) are measured values. The rest are calculated from these using the following expressions;

exit slit dist. = 701.03 - 0.07619*MT

MT = 9201.0 - 13.125*exit slit dist.

A.4 Monochromator Range Change Procedure

Monochromator range changes should only be carried out by experienced personnel. All the beam line valves, stops and masks need to be open through to the experimental chamber. Range changes can only be reliably effected with a stable SR beam which has illuminated the optics for 30 minutes.

Note the latest reliable monochromator settings

Set the MT (mirror translate) cyclometer to the new value. The monochromator mechanism automatically selects the appropriate spherical mirror for each range. The MT drive sometimes sticks. The mechanism outside moves but the mirror carriage inside the monochromator does not. Moving to higher MT numbers (away from the storage ring) the mechanism is positively driven and will not stick. Moving to lower MT numbers (towards the storage ring) the mirror is pulled by a spring and may stick, particularly at extreme positions. Whilst operating the mirror drive the mirror and carriage should be continually watched to ensure that it is moving. If it sticks, back off the MT drive until the mirror moves and alter the MR (mirror rotate) mechanism and try again, however it may require large movements of MR and MT. When the mirror jams the top of the spring which is visible through the side FC38 viewport will be seen to uncoil.

Move the entrance aperture fully out of the beam (fully downwards).

Set the MR (mirror rotate) cyclometer .

Move the GC (grating cyclometer, i.e. grating angle) using either the 'CAL' option on the station software or by setting up the remote stepper motor drive to centralise light by eye on the spherical mirror.

Wind in the aperture rack to select the desired aperture (usually 2mm, i.e. the second aperture) so that the image is central on the spherical mirror.

Set the exit slit micrometer to read between 100 to 150 μm and adjust MR to give optimum drain current either from the tungsten grid I_0 monitor or from a sample in the main chamber. The MR drive has a large amount of backlash. In order to get a reliable reading the drive has to backed off 250 units and then driven close to its expected setting very carefully so as not to overshoot the position. It may require several attempts. For consistency the final position must always be reached whilst driving to higher numbers.

The default settings for the monochromator control program are stored in the file PR:CALIB.DAT. When changing range this file has to be altered. The default settings for other ranges are stored in files PR:CALIB.Rx, where 'x' is the range (i.e. PR:CALIB.R2 is the file for range 2). To nominate a particular file to be the default requires firstly that the existing file be saved by renaming it , i.e. ;

REN PR:CALIB.DAT PR:CALIB.R2 (if the monochromator was set to range 2).

Then simply rename the desired file to be the default file, i.e. for range 3

REN PR:CALIB.R3 PR:CALIB.DAT.

Then when the program is run the status screen should now say "Range = 3" and the CAL command will cause the monochromator to run to the zero order position for range 3.

A.5 Monochromator Exit Slit Zero Calibration

Periodically or when operating at small slit sizes the exit slit zero must be checked. All the beam line valves, stops and masks need to be open through to the experimental chamber. The procedure can only be reliably effected with a stable SR beam which has illuminated the optics for 30 minutes.

Firstly set the slits to give a micrometer reading of 150 μm.

Optimise the zero order light using the calibrate facility.

Set the photon energy to 140 eV or the maximum of whichever range is in use.

Record the drain current either from the I_0 vessel or from a sample in the main chamber at several micrometer readings, e.g. 50, 100, 150, 200, 250 μm.

Plot drain current vs. micrometer reading and work out the intercept.

Set the micrometer to the intercept value and press the zero button.

The exit slit zero should now be correct.

For consistency it is best to set the micrometer to the desired value whilst driving to higher numbers. If a lower value is needed go back to zero and approach the setting whilst driving to higher numbers.

A.6 Filter Settings

The linear drive which moves the filter assembly across the photon beam requires setting to a predetermined position for each filter or the beam may be clipped by the filter mount. The position is measured in mm across the inside faces of the linear drive's FC38 flanges. Setting to the nearest mm is sufficient.

Filter	Useful range eV	Position mm
none	-	140 (fully out)
Si	72 - 99	86
Al	36 - 72	62
Al/Mg/Al	25 - 49	38 (fully in)

A.7 Resolution vs. Exit Slit Figures

These are Gaussian fits to experimental data i.e.;

$$\sigma = K0 + K1 \times e^{-(\frac{S}{K2})^2}$$

where σ is the monochromator FWHM resolution in meV and S is the exit slit micrometer reading in μm. The curves and the data points are shown in figure 12 in section 2.4.5. The Gaussian curve fit is simply an aid to interpolation between data points and has no physical significance.

Photon Energy, eV	K0	K1	K2
80	332.4	-244.9	789.1
100	2290	-2192	1734
120	2476	-2375	1407
140	5701	-5589	1635
160	3407	-3300	824.1

A.8 Fixed Bandpass Settings

These are fits to points linearly interpolated from actual data and fitted to a simple exponential i.e.;

$$S = K0 + K1 \times e^{-E \times K2}$$

where S is the exit slit micrometer reading in μm and E is the photon energy in eV. The curves are shown in figure 14 in section 2.4.5. The exponential curve fit is an aid to interpolation between data points and has no physical significance.

Bandpass meV	K0	K1	K2
150	50.09	2812	0.02509
200	121.1	5477	0.02983
250	136.1	7604	0.03063
300	153.3	9650	0.03116

A.9 Stability Of Energy Calibration Throughout A Fill

The monochromator is calibrated by checking the encoder reading for zero order and writing the new number to a calibration file PR:CALIB.DAT. The monochromator driving programme then calculates the angle, ϕ, that the grating has to be moved from zero order from

$$\phi = \sin^{-1}\left[\frac{N * k * 12398.5 * 10^{-7}}{2 * E * \cos\theta}\right]$$

where N is the line density of the grating (l/mm), k is the order of diffraction, θ is the zero order angle and E is the required energy in eV. The grating angle drive encoder value, POSN, is then calculated from

$$POSN = c * L_v\left[\sin(\tau_n + \phi) - \sin(\tau_n)\right] + datum$$

where c is the number of encoder units per mm, L_V is the length of the lever arm, τ_n is the angle of the lever arm (with respect to horizontal) in zero order for range n and *datum* is the encoder reading for zero order for range n.

Obviously if *datum* changes during a fill, then the encoder reading for a particular energy will also change.

In Feb. '86 the drift with time of the zero order encoder value was recorded. The general trend was to decrease by about 20 encoder units in 1 to 2 hours from initial readings and thence to slowly increase. This behaviour is not consistent; as improvements are made to the machine and to optics cooling and stability this drift is decreased.

Plotted in figure 26 is the energy in eV per encoder unit as a function of energy for the three ranges and for the 632 l/mm grating. The higher line density grating reduces the effect of zero order drift but it still should be checked routinely where precise energy calibration is required.

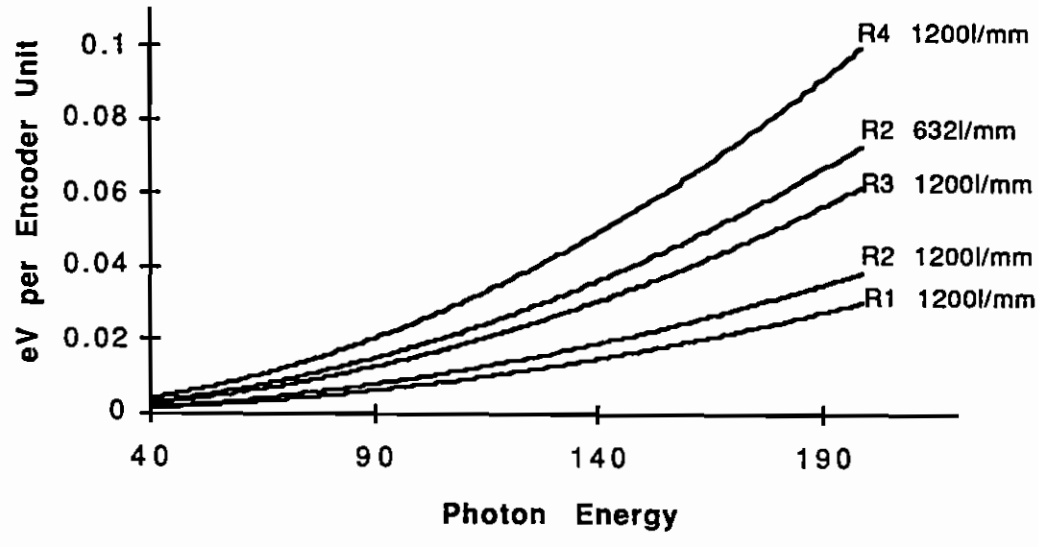

Figure 26 Stability of energy calibration throughout a fill

A.10 Second Order Content

The following tables give the percentage of second order in the monochromator output for the blazed and lamellar gratings. These data are not corrected for the change in photoemission cross-section with photon energy; corrected data would be substantially higher.

1. Blazed grating

Photon Energy eV	Range 2	Range 3	Range 4	Range 2 re-coated
20			3.2	
30			4.7	
40	11.8	17.5	39.4	29.3
50			9.3	16.6
60	5.4	26.7	0.01	14
70	3			8.6
80	4.2	0.04		4.6
90	2.4			2.5
100	0.78			0.6
110	0.41			
120	0.41			
130	0.283			
140	0.17			
150	0.02			

2. Lamellar grating

photon energy eV	range 2	range 3	range 4
30			30.6
35			66.1
40			64.8
45		87.5	28.4
50		65.2	11.5
52	38.8		
55		54.6	2.44
60	31.6	27.4	
65		10.6	
70	9.18	1.8	
80	3.47	0.062	
90	1.35		
100	0.39		

A.11 Technical Performance

Beam Size At Sample;
3 mm horizontal by 0.3 mm vertical approximately.

Sample manipulation;

Temperature;	heating to 1000 K
	cooling to 110 K
Rotation;	Polar 360°
	Azimuthal 180°
Movement;	X (in plane) ±12.5 mm
	Y (in plane) ±12.5 mm
	Z (out of plane) 165 mm

Analysers;

HA100;
VSW Scientific Instruments model; HA100 (MCD)
100 mm mean radius hemispherical electrostatic energy analyser
Using the HAC500 controller either electrons or ions can be analysed
Lens type; 14D
Detection; multi channel (16 channels simultaneously)
Kinetic energy range; 0 - 5000 eV
Pass energies; 1 - 90 eV
Rotation; none (fixed at 90° to beam)
Angular acceptance; variable, <5° half angle
Resolution; 1.5% of PE (best observed = 38 meV @ 1 eV PE)
Count rate is approximately proportional to pass energy

HA50;
VSW Scientific Instruments model; HA50
50 mm mean radius hemispherical electrostatic electron energy analyser
Detection; single channel (channeltron)
Kinetic energy range; 0 - 300 eV
Pass energies; 1 - 50 eV
Rotation; 270° in plane, 80° out of plane
Angular acceptance; ~ 2° half angle
Resolution; 1.0% of PE (best observed = 14 meV @ 1 eV PE)
Count rate is approximately proportional to pass energy

CMA;
PHI model; 15-255g
angle integrating double pass cylindrical mirror electron energy analyser
Detection; single channel (channeltron)
Kinetic energy range; 0 - 2000 eV
Pass energies; 5 - 200 eV
Gun energy range; 100 - 5000 eV
Rotation; none (fixed at 90° to beam)
Angular acceptance; 6° half angle at ~40°, 360° annulus
Resolution; with 4 mm aperture (XPS) 2.0% of pass energy
with 1 mm aperture (AES) 1.2% of pass energy
Count rate is approximately proportional to pass energy